

Original Article

# IoT Based Real Time Monitoring of PV Sourced Battery with High Gain Boost Integrated Zeta Converter for EV

R. Ramani<sup>1</sup>, A. Nalini<sup>2</sup>

<sup>1,2</sup>Department of Electrical and Electronics Engineering, Dr. M.G.R. Educational and Research Institute, Tamilnadu, India.

<sup>1</sup>Corresponding Author : [ramanikamal11@gmail.com](mailto:ramanikamal11@gmail.com)

Received: 22 September 2023

Revised: 25 October 2023

Accepted: 20 November 2023

Published: 02 December 2023

**Abstract** - The advancement of science and technology has resulted in a wide range of electric energy sources such as solar, hydro, wind, etc. Electricity is transmitted from these energy sources to metropolises, companies and home environments for life and work. Modern technologies rely heavily on electrical energy. However, monitoring and controlling grids is essential to ensure services are available promptly. Accordingly, this paper proposes a Photovoltaic (PV) system for effective energy management and the Internet of Things (IoT) to make the system safe, reliable and energy-efficient. In the proposed work, for charging an Electric Vehicle (EV) battery, the voltage created by the PV system is enhanced by adopting a high-gain Boost-Zeta converter. To control the converter effectively, the Improved Moth-Flame Optimization-Proportional Integral (IMFO-PI) controller approach is utilized to attain stabilized converter voltage. This converter has a single switch design and can offer increased voltage gain at lower duty ratios. Furthermore, it possesses the advantages of non-inverted output, enhanced power factor, reduced input current distortion, minimal work current ripple, and a wide output power range. Similarly, the IMO method prevents local optimums by combining well-organized exploration and exploitation with fast convergence. With the aid of a battery converter, extra energy produced by a PV system is stored in batteries. The active conversion of DC voltage to AC occurs with Single Phase Voltage Source Inverter (1 $\Phi$ VSI)'s support for grid supply. Furthermore, the LC filter attached to the grid reduces the harmonics and provides improved AC supply to the grid. Additionally, the IoT connected to the system monitors the State of Charge (SOC) of the EV battery, Current and voltage from the PV system to ensure reliable and adequate supply. Finally, the entire proposed system implemented with MATLAB Platform is used to verify its performance.

**Keywords** - PV, IoT, EV battery, High gain boost integrated Zeta converter, PI-IMFO, SOC.

## 1. Introduction

Electric Vehicles (EVs) are becoming increasingly common as petrol costs steadily increase. Due to these factors, some vehicle manufacturers have been searching for clean energy sources to fuel. The usage of electrical sources is helpful for the environment because emissions are decreased. Photovoltaics (PVs) also give substantial advantages in energy conservation and environmental protection [1, 2]. Increasing costs and deficits of fossil fuels have led to the adoption alternative energy sources.

Renewable Energy Sources (RES), such as PV-based energy generation, are becoming increasingly popular in numerous applications, particularly in EVs [3]. DC-DC converters derive an appropriate voltage from solar panels, considering price, effectiveness and maximum solar radiation variables. A DC-DC converter with an increased gain voltage ratio achieves large voltage outputs by combining inductance and capacitance configurations and connecting the lower-voltage PV panel to the high-voltage DC connection [4]. Due to significant conduction loss, increased voltage stress, and

diode reverse recovery issues; traditional boost converters are ineffective for increasing PV output voltage [5]. Buck-boost converters can convert voltages up and down, although their efficiency has limitations because of interrupted input current [6-8]. To improve performance and voltage moderation, Cuk and Single Ended Primary Inductance Converters (SEPIC) with low switching losses are utilized; however, because of their considerable input and output inductors and lack of rapid speed up/down voltage, these converters are not recommended [9, 10]. Although a Zeta converter has characteristics comparable to a buck-boost converter, it possesses the benefit of producing non-inverted output.

It has a more fantastic duty ratio range than any other converter. However, it has more excellent input voltage ripple content. To address the abovementioned issues, this paper suggests a high-gain boost integrated Zeta converter, which provides maximum voltage gain with reduced ripple contents. Most EVs use lithium ion batteries, which are much simpler than lead-acid batteries. It has a six to ten times higher life cycle and uninterrupted power than a lead acid battery.



Two frequent factors that shorten the life cycle of lithium ion batteries are overcharging and severe discharges. In contrast, the size and design of EV batteries often result in a limited driving range. The security of present battery systems is now one of the most significant factors restricting the usage of EVs [11]. For instance, overcharging a battery significantly shortens its lifespan and poses serious safety risks, including fire [12, 13]. Therefore, it is essential to have a battery monitoring system in electric vehicles that warns the driver of the battery's condition to prevent the abovementioned problems. The earlier battery monitoring system only observed and recognized the battery's state and informed the person through the battery indicator on the EV.

Because of improvements in alerting system planning, manufacturers and consumers commonly receive notifications concerning battery status through the Internet of Things (IoT) technologies. Proportional Integral (PI) controllers' capability, wide range stability margin, and longevity make them popular industrial controllers [14]. Nevertheless, network variability and elemental variations affect these PI controllers. As a result, more excellent PI controller fine-tuning is required, which is considered a possibility for regulating grid-connected solar energy projects. In [15], the Cuckoo Search Algorithm (CSA) is especially helpful in global search since it is considerably more effective than any other random-walk-based randomized method. Particle Swarm Optimisation (PSO) [16], Genetic Algorithm (GA) [17] and Gray Wolf Optimization (GWO) [18] algorithms are used to modify the gain settings of the PI controller [19]. These approaches offer quick convergence and precise findings. Nevertheless, the previously mentioned approaches have disadvantages, including a slow convergence rate and inadequate convergence precision.

Computationally costly weak convergence in the refined search step and a penchant for rapid and premature convergence in the mid-optimal point. Improved moth flame optimization algorithm avoids local optimums with effectively organized exploration and exploitation, which overcomes these restrictions. It is reliable, easy to use, and suitable for challenging optimization positions. Due to their characteristics, such as low current harmonics and bidirectional energy flow capability, single-phase voltage source inverters [20] have become highly popular in grid-connected PV systems. The PI controller constitutes one of the controllers examined for managing the stable state and transient response of grid-tied inverters. This Voltage Source Inverter (VSI) injects AC into the grid at a specific frequency and with low THD using a filter. An effective PI-controlled 1 $\Phi$ VSI provides reduced grid current THD, reduced steady-state error, durability, and quick dynamic response. However, based on the literature reviews, the intended control and converter approaches are unstable for functioning smoothly. Because of their lack of high-speed up/down voltage, these converters require the help of a large coupling capacitor to

accomplish good MPPT working. Furthermore, the optimized PI controllers have issues such as failing to converge as an efficient solution at local optimal locations and having a poor convergence rate. Henceforth, the main contribution of our work is summarized as follows:

- This article highlights a PV-fed EV battery-based IoT monitoring system that efficiently monitors parameters like PV voltage, current and State of Charge (SOC).
- A novel High-gain Boost-ZETA converter has been developed to maximize solar panel voltage.
- An innovative, improved moth flame-optimized PI controller sustains a high-efficiency constant voltage supply.
- IoT display visualizes battery parameters such as PV voltage, current, and SOC.

The entire system is executed in the MATLAB platform, and the results are used to improve the system's performance.

## 2. Related Works

Farzam Nejabatkhah et al. [21] have proposed a novel three-input boost converter for hybrid PV/FC/battery power systems. According to the computational outcomes, the converter control framework delivers excellent transient and stable state responses for the converter following varied step variations in PV power production and load situations. However, this converter is incapable of increasing the input voltage. Francarl Galea et al. [22] have presented an outstanding efficacy broad input-ranging isolated Cuk converter architecture for grid-linked regenerating active loads. The resultant voltage is possibly higher than the input voltage. The primary limitation of this converter is substantial current stress on the switch.

Patan Javeed et al. [23] demonstrate a SEPIC Converter for developing a small power LED application. Compared to an electrolyte capacitor, this enhances the overall performance of the LED driver. Nevertheless, it is more complicated, resulting in a more susceptible structure. S. Saravanan et al. [24] proposed using a fuzzy logic controller to evaluate and optimize a transformerless, highly effective Zeta converter for clean energy usage. The architecture of this converter is quite simple, which facilitates the management of operations and minimizes switching and conduction losses. On the other hand, the output capacitor's charging current is inconsistent, leading to a higher capacitor size and EMI concerns.

## 3. Proposed System Description

A grid-incorporated PV system with an EV battery monitoring system is proposed in this article to track the parametric data like  $V_{PV}$ ,  $I_{PV}$  and SOC. The suggested system comprises the main components: EV Battery, high gain Boost integrated Zeta converter, IMFO-PI controller, LC filter and 1 $\Phi$ VSI. The overall proposed system is represented in Figure 1.

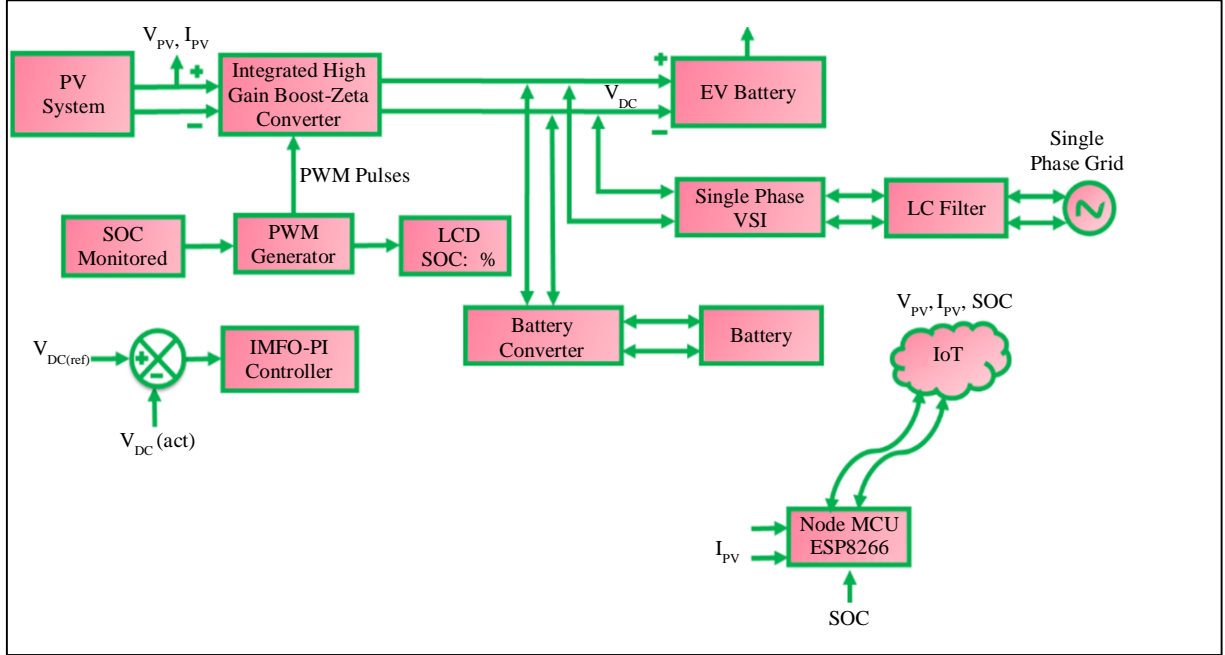


Fig. 1 PV-fed EV battery based IoT monitoring system

Specifically, the input to the high gain boost integrated Zeta converter and the PI controller are the output Voltage ( $V_{PV}$ ) and Current ( $I_{PV}$ ) from the PV panel. The controller requires a mechanism for optimization to achieve optimal results.

PI controller factors  $K_p$  and  $K_i$  are optimally fine-tuned through the use of the Improved Moth Flame Optimization (IMFO) algorithm. The optimized PI controller is simulated to provide stabilized voltage and current control to establish the output duty ratio for the high gain boost integrated Zeta converter.

To maximize the converter's power output, the suggested controller controls its output voltage and current. Moreover, the single-phase VSI, under the influence of the PI controller, receives constant DC link voltage produced by the PV system. And also, the 1 $\Phi$ VSI assures smooth functioning with minimized harmonics. IoT is employed for tracking significant factors such as  $I_{PV}$ ,  $V_{PV}$  and SOC of the battery system that impacts the PV system's functioning.

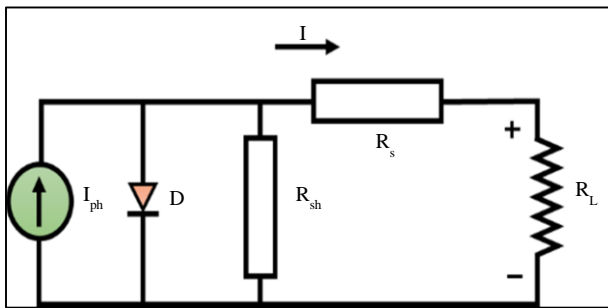


Fig. 2 Solar system

## 4. Proposed System Modelling

### 4.1. PV System Modelling

Electricity produced by a PV system linked to the grid is transmitted to the grid for direct transmission, distribution and consumption. In broad terms, a PV system's output properties are influenced by its operation temperature and solar cell irradiance. The analogous PV system circuit diagram is presented in Figure 2. Current and voltage expressions are provided by,

$$I_{ph} = I_D + I + \left(\frac{V_D}{R_{sh}}\right) \quad (1)$$

$$V = V_D - (I * R_s) \quad (2)$$

Where the diode current  $I_D$  is,

$$I_D = I + (e^{(V_D/V_T)} - 1) \quad (3)$$

Examining irradiance variation and temperature influence is made more accessible by (1) and (2), which forecast the properties of current and voltage.

The voltage in an open circuit fluctuates less when the irradiance changes, while the short circuit current varies significantly. These factors negatively affect the PV system's output voltage, necessitating an effective DC-DC converter to increase the PV system's output.

### 4.2. High Gain Boost Integrated Zeta Converter Modelling

A solar panel's output voltage is typically low. Appropriate converters must be utilized to raise their voltage level and fulfil the varying characteristics.

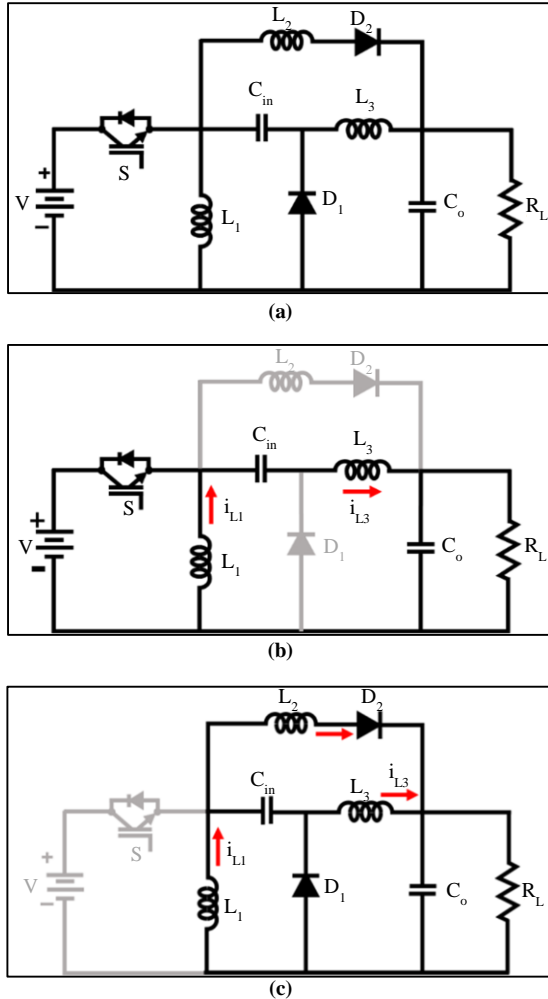


Fig. 3 The suggested circuit diagram (a) High gain boost integrated Zeta converter, (b) Phase 1, and (c) Phase 2.

An innovative high-gain Boost integrated Zeta converter is used in this work to improve the conversion process, resulting in a regulated output voltage without polarity inversion. A high-gain output converter minimizes the price and quantity of PV panels necessary for producing electricity. Figure 3(a) illustrates the circuit diagram for the suggested high gain Boost integrated Zeta converter, and the functioning of the recommended converter configuration is shown in Figure 3(b) (switch  $S$  is active) and Figure 3(c) (switch  $S$  is disabled).

When  $S$  is turned on in phase 1,  $L_1$  saves power provided by the source  $V$ ;  $C_{in}$  transmits energy to  $L_3$ . The separate diodes  $D_1$  and  $D_2$  are turned off in this case, and the power delivered to the loads is given by  $L_3$  and  $C_o$ . When  $S$  is turned off in phase 2, the collected power in the inductors is transferred to the capacitors  $C_{in}$  and  $C_o$  via the diodes  $D_1$  and  $D_2$ . The incorporation of the IMFO-PI controller improves the performance of the high gain Boost integrated Zeta converter. The complete outline of the intended optimized controller is described in the upcoming section.

### 4.3. Improved Moth-Flame Optimized PI Controller

#### 4.3.1. PI Controller

The PI controller is among the numerous highly suitable controllers for various fields. The utilization of these controllers necessitates the use of their modifying factors to produce the desired results. As a result, it is vital to select an approach that is quick and simple to implement. These control parameters ( $K_P$  and  $K_i$ ) ought to be identified. The controlling structure for the PI controller is shown in Figure 4.

Virtually any operation capable of controlling motion, aerospace, or slow to rapid systems has been handled with PI controllers. Due to fluctuations in operational points and system dynamics modifications, PI controllers must be adjusted frequently. Where the  $K_P$  indicates proportional gain, and  $K_i$  means integral growth.

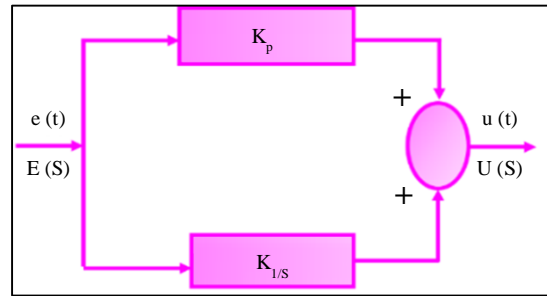


Fig. 4 PI controller

Adjusting PI controller parameters is difficult when uncertain, non-linear and complicated systems are considered. To tackle these problems, this paper proposes an effective optimization algorithm, namely the IMFO algorithm, to improve the performance of the PI controllers.

#### 4.3.2. IMFO Algorithm

The MFO technique is a population-based SI method; commonly, it simulates the behaviours of moths as they travel towards light sources. The moths follow an uninterrupted path with a fixed angle towards the real-light source (moon), known as transverse orientation.

The moths and flames are included as outcomes in this method. The initial distribution of moths over the search area is random, and their locations are recorded in an  $N \times D$  dimensional matrix  $M$ . As demonstrated below, the  $M$  fitness value is computed and stored in an array  $OM$ .  $OM$  represents the current position of the moths' fitness.

$$M = \begin{bmatrix} m_{1,1} & m_{2,2} & \dots & \dots & m_{1,d} \\ m_{2,1} & m_{2,2} & \dots & \dots & m_{2,d} \\ \vdots & \vdots & \dots & \dots & \dots \\ m_{n,1} & m_{n,2} & \dots & \dots & m_{n,d} \end{bmatrix} \quad (4)$$

During the procedure of optimization, every moth  $M_i(t)$  in the present iteration  $t$  travels close to the appropriate flame  $F_j$

employing an exponential spiral distinct by (5), where  $Dis(t)$  is determined using (6),  $b$  represents  $k$  and logarithmic spiral shape is a randomly generated value between  $(-1, 1)$ .

$$M_i(t) = Dis_i \cdot e^{bk} \cdot Cos(2\pi k) + F_j(t) \quad (5)$$

$$Dis(t) = |F_j(t) - M_i(t)| \quad (6)$$

Equation (7) is used in this method to calculate the amount of flames:

$$flame_{no} = round\left(N - t \times \frac{N-1}{MaxIt}\right) \quad (7)$$

Where  $t$  presents iteration, the maximum number of iterations is represented by  $MaxIt$ , and  $N$  is the number of search agents accordingly. The MFO algorithm is a powerful problem-solving tool commonly used in real-world optimization situations. However, the primary shortcomings of MFO and its proposed adaptations are excessive convergence, an impasse in localized optimum, poor population diversity, and insufficient integration of exploration and exploitation.

As a result, in this case, the improved MFO algorithm is presented to overcome the drawbacks of the classical MFO. To address the weaknesses of the traditional MFO algorithm, the suggested IMFO algorithm is enhanced with an Adapted Wandering Around Search (AWAS) and moth memory structure strategy. Each moth in the proposed method must only update its position with the specific flame that corresponds to it, preventing the system from settling on a local optimal value. This considerably improves the algorithm's ability to perform a global search.

In the IMFO method, confined moths are found by contrasting their present position's fitness (OM) with the highest possible observed flame fitness (Fbest). The AWAS method is used to potentially permit encased moths from their local optimal through carrying out a few random brief flight movements, which also helps mitigate early convergence. If every moth's present location does not correspond superior to its recall, the moth is regarded to be surrounded.

Additionally, by restricting moths' flying range ( $fl$ ), this parameter establishes an appropriate equilibrium between exploitation and exploration. If the resulting fitness value exceeds Fbest, it replaces a former position and fitness value. The moth memory system is inspired by how moths recollect their natural experiences, as specified in Description 1.

Furthermore, in condition 2, the AWAS technique is added to potentially release confined moths from local optimal conditions and reduce early convergence.

Algorithm 1: IMFO Pseudocode
Input maximum iteration (MaxIt), No. of moths (N) and size of dimension (D)
Output: The most effective flame location and its fitnessrating
Begin
Deploying M moths at randomised in a D – dimensional search area
Determining moth's fitness (OM)
Set t = 1
OF ← sort (OM).
F ← sort (M).
Considering criterion 1, define the moth memory Mbest and Fbest.
While
F and OF are being updated with the finest N moths from M and current F
Updating flame_no using equation (7)
For i = 1: N
Computing the distance between moths $M_i(t)$ and $F_i(t)$ using equation (6)
Updating the location of $M_i(t)$ using equation (5).
Computing the fitness value $OM_i(t)$ .
If $Fbest_i(t) < OM_i(t)$
Selecting a random moth $Mr(t)$ .
Updating the position of $M_i(t)$ using AWAS defined in condition 2
Updating the fitness value $OM_i(t)$
End if
Updating the moth memory $M_i$ using Condition 1.
End for
Updating the position and fitness value of the global best
t = t + 1
End while

Algorithm 1 and Figure 5 correspondingly demonstrate the suggested I-MFO's pseudocode and flowchart. Description 1: Assume  $Mem = Mem1, Mem2, \dots, Mem_i, \dots, MemN$  is a finite set of N moths' experiences.  $Mem_i = (Mbest_i, Fbest_i)$  denotes the moth of memory  $M_i$ , whereas  $Mbest_i$  is the best location that  $M_i$  achieved thus far, and  $Fbest_i$  is  $Mbest_i$  fitness value.  $Mbest_i(t=1) \leftarrow M_i(t=1)$  and  $Fbest_i(t=1) \leftarrow OM_i(t=1)$  are the best positions in the first iteration  $t$ .  $Mbest_i(t > 1) \leftarrow M_i(P)$  and  $Fbest_i(t) \leftarrow OM_i(P)$  for the remaining iterations, resulting in  $OM_i(P) < Fbest_i(t)$ ,  $P = 2, \dots, t$ . Equation (8) expresses the moth memory structure.

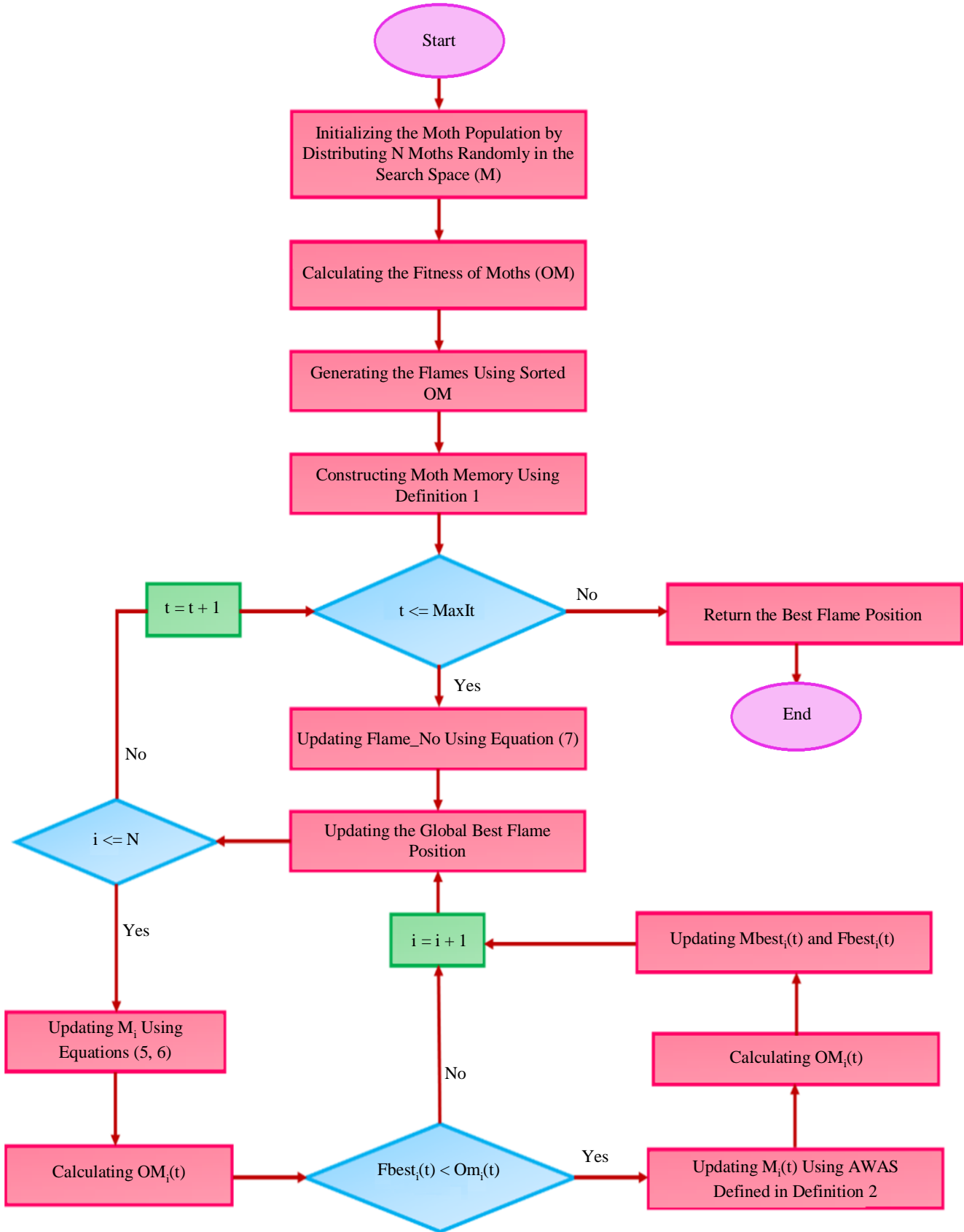


Fig. 5 Flowchart for the proposed algorithm

If  $t = 1$  then  $F_{best_i}(t) \leftarrow OM_i(t)$  and  $M_{best_i}(t) \leftarrow M_i(t)$   
 If  $t > 1$  then  $F_{best_i}(t) \leftarrow OM_i(P)$  and  $M_{best_i}(t) \leftarrow M_i(P)$  (8)

Such that as  $s \in \{2, \dots, t\}, OM_i(s) < OM_i(P)$

Description 2 (AWAS approach): Assume  $TM(t) = \{M1, \dots, Mi, \dots\}$  as a finite collection of moths caught in iteration  $t$  where  $Mi$  is unable to control its  $Memi(OM_i(t) > F_{best_i})$ .

Trapped moth  $Mi(t + 1)$  is then freed from the local optimal condition by Equation (7), while  $F_{gbest_j}(t)$  is the  $j$ th global finest flame dimension,  $r_i$  is a random number between  $(0, 1)$ , and  $fl_i(t)$  is the probability of a randomized moth location.

Equation (8) computes flight length  $fl_i(t)$  for moth  $Mi$ , while  $d1$  and  $d2$  are user-defined,  $NF$  is the amount of flight generated randomized in  $[1, D]$ , and  $q$  is the present flight number. Indeed, integrating the AWAS approach with randomized  $NF$  offers a benefit that allows the trapped moth  $Mi$  to be transferred to an improved location.

$$M_{ij}(t + 1) = F_{gbest_j}(t) + r_i \times fl_i(t) \times (M_{rj}(t) - M_{ij}(t)) \quad (9)$$

$$fl_i(t) = \delta_1 - q \times \left(\frac{\delta_2}{NF}\right) \quad (10)$$

With the implementation of the IMFO algorithm, the PI controller parameters ( $K_p, K_i$ ) are tuned optimally. In addition to the IMF-optimized PI controller, the working functionality of the high gain Boost integrated Zeta converter was enhanced.

#### 4.4. Single Phase VSI Modelling

Low-power solar energy systems are frequently linked to the AC grid with  $1\Phi$  inverters. Using an LC filter, the VSI effectively reduces harmonics, and the associated circuit design is presented in Figure 6. The traditional PI controller, which lowers the actual and reference power values variance, synchronizes the grid.

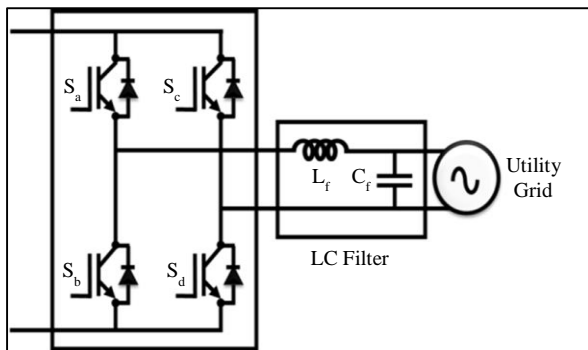


Fig. 6 Circuit diagram of  $1\Phi$  VSI

The results are turned into the proper pulses and sent to the VSI. The VSI transforms DC voltage from the DC link into AC form for grid injection.

The VSI functions as a current source rather than a voltage source while in grid-linked mode. The inverter introduces higher-quality power into the grid at manageable voltage, frequency, and phase angle changes according to the synchronization.

As an outcome, the output in the  $1\Phi$  grid is an excellent integrated voltage. The suggested approach effectively presents a grid-related PV system with high gain Boost integrated Zeta converters and an IMF-optimized PI controller as an efficient way to generate outputs of higher quality.

#### 4.5. PV Fed EV Battery System Parameter Monitoring Using IoT

The value of IoT-based parameter tracking for PV systems lies in its potential to optimize system reliability and effectiveness. PV systems are a primary renewable energy source, and their efficacy is vital in maintaining a dependable and environmentally friendly power supply.

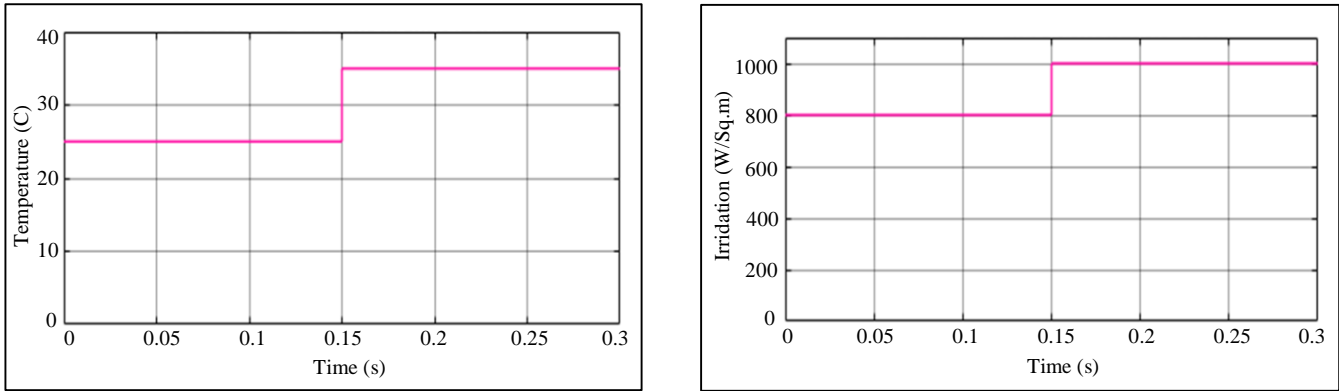
IoT-based factor observation enables real-time evaluation of parameters like voltage, current, and SOC. In addition, IoT-based parameter observation allows for remote management and monitoring of PV systems, helping operators to operate and maintain the system from a centralized location. As a result, the requirement for on-site visits is decreased, resulting in time and resource savings.

### 5. Results and Discussion

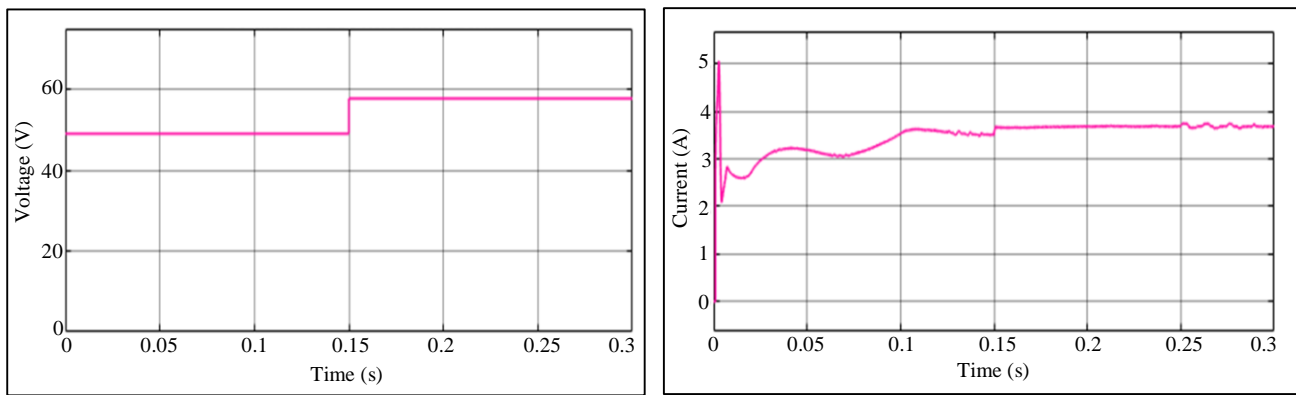
In this paper, a unique high-gain boost integrated Zeta converter is put forward, combined with a reliable IMF-optimized PI controller, to increase the reliability of a grid-linked PV system. The suggested PV system connected to the power grid design is continuously tracked utilizing IoT to enhance overall system reliability and performance. The parameters in Table 1 are used for developing the grid-tied PV system simulation model.

Table 1. Parameters specification

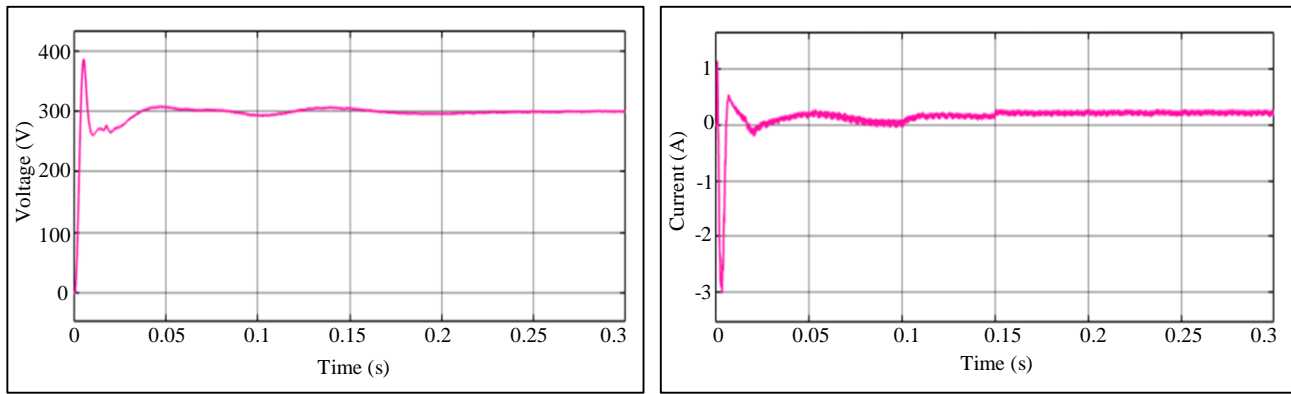
Parameters	Values
PV system	
Total count of panels	8 panels, 250 W
Power	2000 W
High gain boost integrated Zeta converter	
Switching frequency $f_s$	10 kHz
$L_1, L_2, L_3$	1 mH
Output capacitor $C_o$	220 $\mu$ F
Input capacitor $C_{in}$	750 $\mu$ F



(a) (b)  
**Fig. 7 Waveforms of solar panel (a) Temperature, and (b) Irradiation.**



(a) (b)  
**Fig. 8 Waveforms of the solar panel (a) Voltage, and (b) Current.**



(a) (b)  
**Fig. 9 Output waveforms of high gain boost integrated Zeta converter (a) Voltage, and (b) Current.**

To assess the efficacy of the suggested strategy for tackling PV system intermittency, a temperature variation of 0.15s is imposed, as illustrated in Figure 7(a). At this moment, the temperature rises sharply from 25°C to 35°C. Similarly, solar irradiation changes from 800 W/Sq.m to 1000 W/Sq.m, as illustrated in Figure 7(b). Figure 8 shows how temperature change at 0.15s affects the PV system's current and voltage.

The voltage rises from 50V to 58V, the amount of current rises to 3.8A, and the current remains stable at 0.15s. Figure 9 depicts the waveform indicating the resultant voltage derived from the high gain boost integrated Zeta converter. From the waveform demonstration, it is clear that a constant converter voltage of 300V is obtained. Likewise, with small distortions, the current became a stable value of 0.3 after 0.18 sec.

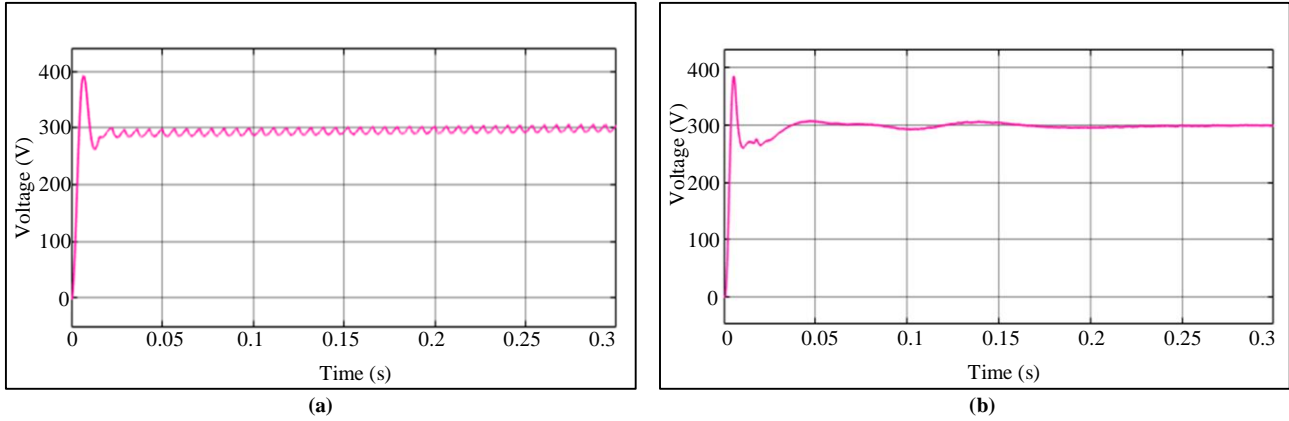


Fig. 10 Output voltage waveforms of proposed converter (a) Utilizing PI controller, and (b) Utilizing IMFO-PI controller.

Figure 10 shows the converter's output utilizing an IMF-optimized PI controller. Unlike the typical PI controller, the suggested IMF-optimized PI controller maintains a steady voltage. Within 0.26 seconds of settling, a consistent and constant voltage of 300V is obtained. At 0.02sec, the converter's output voltage remains stable, and a continuous value of 300V is obtained. The battery voltage waveform in Figure 11(a) demonstrates that a constant voltage of 12V remains maintained. SOC, or the volume of energy accessible

through the battery compared to its capacity, is a significant factor for BESS management. The battery current waveform is in Figure 11(b), and the current magnitude from the battery is 2.1A. The battery's SOC is 60%, as shown in Figure 11(c), and the charging and discharging operation is initiated based on this value. Figure 12 displays the grid current and voltage, showing that the grid is supplied with a constant voltage of 230V and 5A. At magnitude 5A, grid current requires 0.05sec to stabilize.

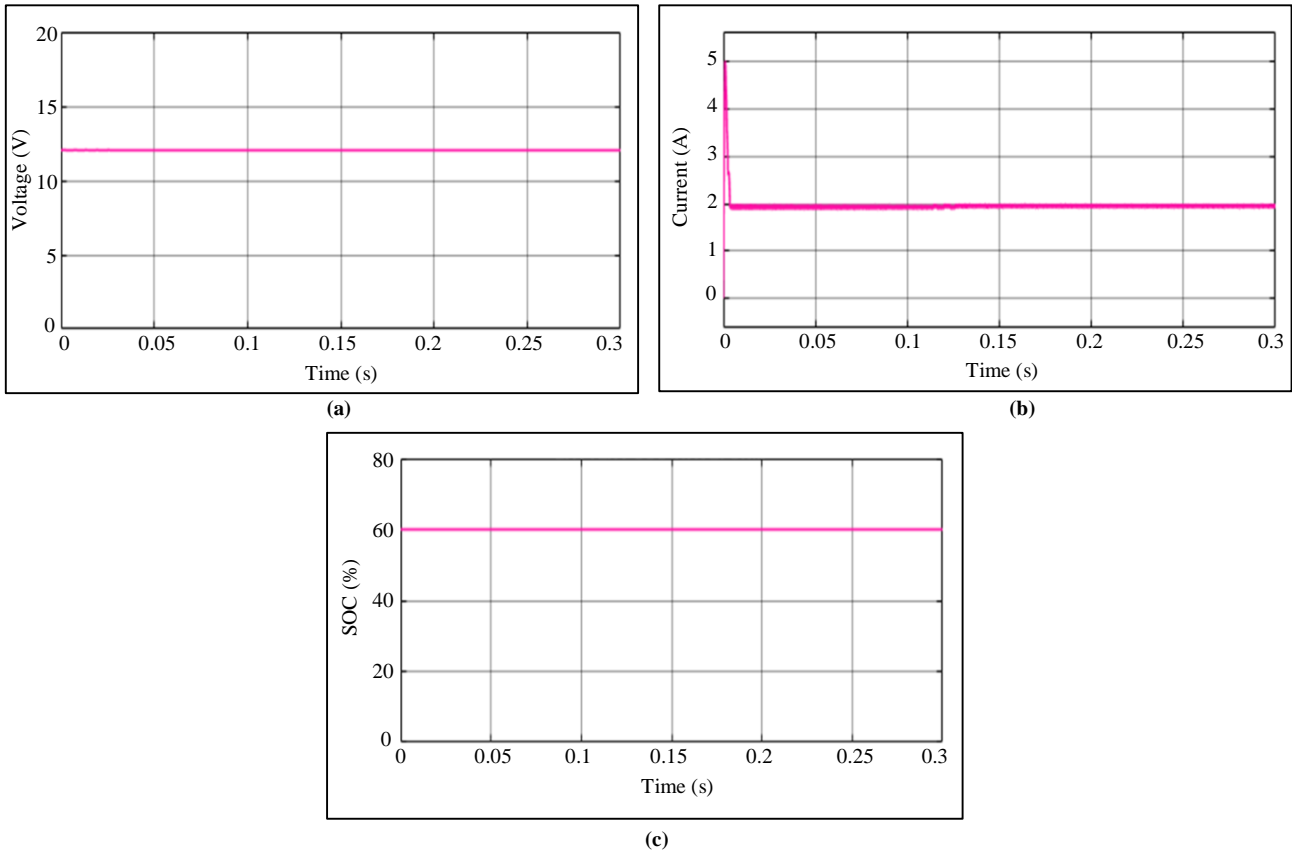


Fig. 11 Waveforms of EV battery (a) Voltage, (b) Current, and (c) SOC.

Figure 13 depicts waveforms demonstrating the real and reactive power of the 1 $\phi$  grid. At 0.1sec, real power stays steady at 780W, while the magnitude of reactive power declines to a minimal value after attaining a high point of 800W at 0.05sec. Figure 14 illustrates the waveform for the power factor, which shows that the unity power factor is achieved after 0.01 sec. Figure 15 depicts the suggested system's IoT viewpoint.

As shown in Figure 15, IoT is utilized to continuously monitor characteristics such as solar panel output current, voltage, and battery SOC. Sensors, such as current and voltage sensors, are used to collect reliable information about variations in these variables. Furthermore, the MySQL Cloud service collects, manages, analyses, and shows the obtained data. Figure 16 depicts the suggested converter THD value of 2.25% with minimized harmonics.

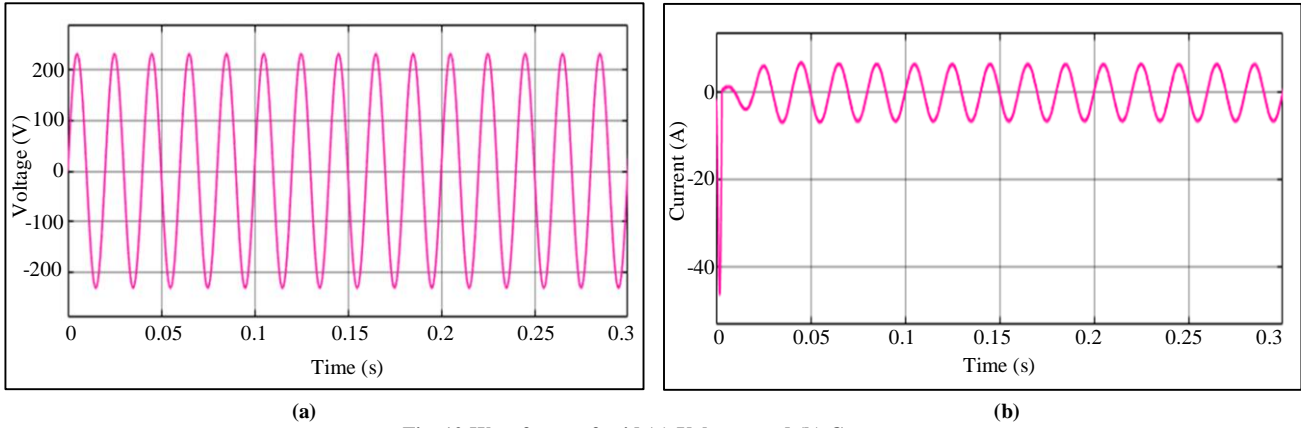


Fig. 12 Waveforms of grid (a) Voltage, and (b) Current.

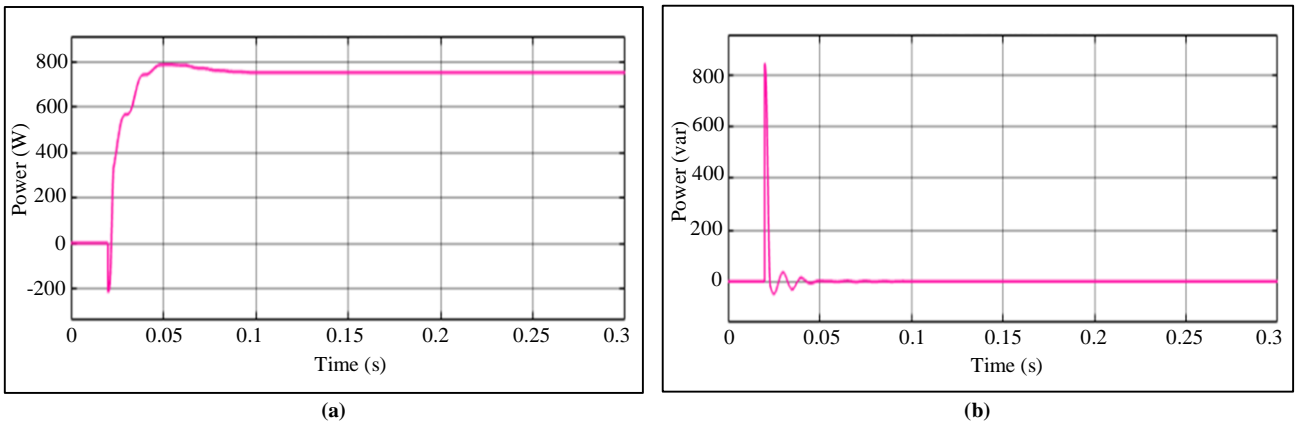


Fig. 13 Waveforms of (a) Real power, and (b) Reactive power.

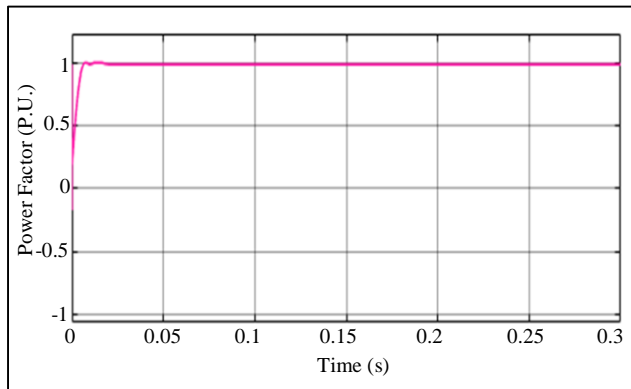


Fig. 14 Power factor waveform

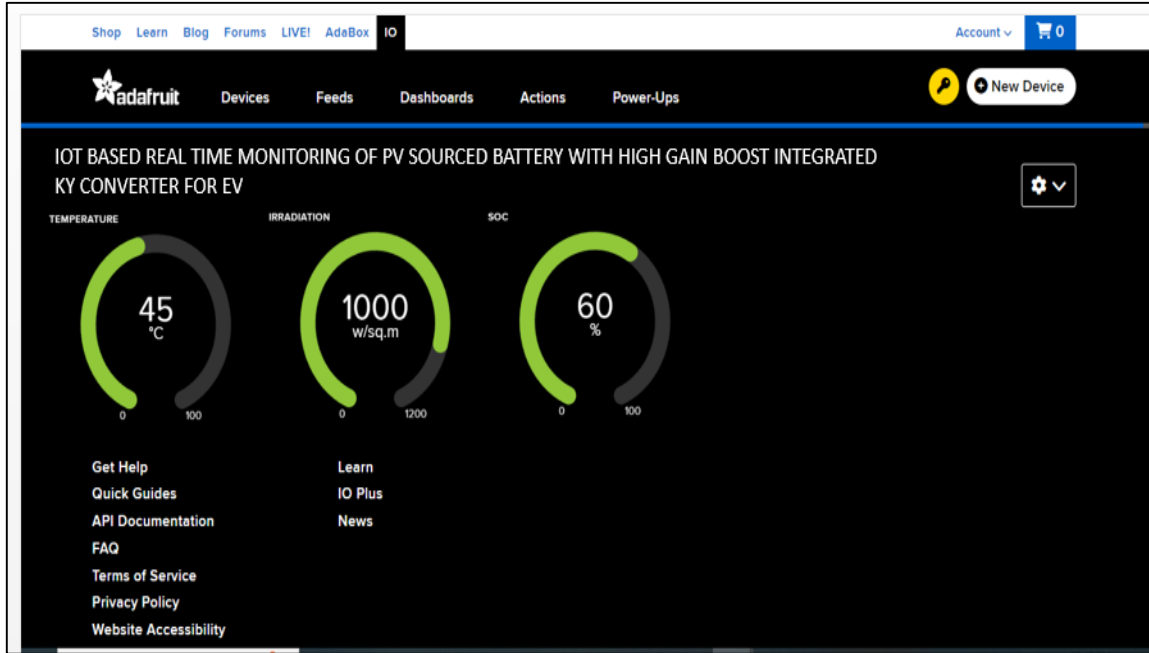


Fig. 15 IoT view

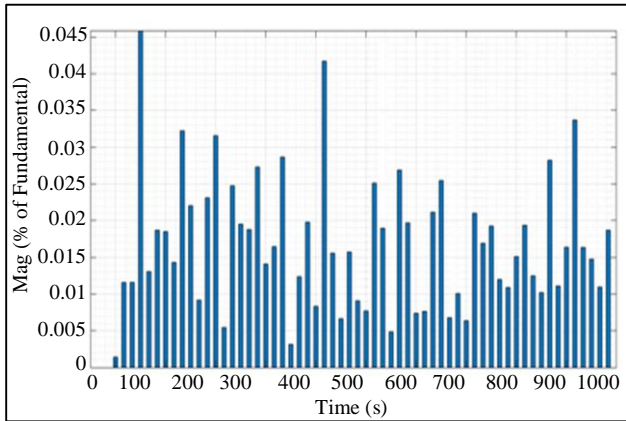


Fig. 16 THD waveform

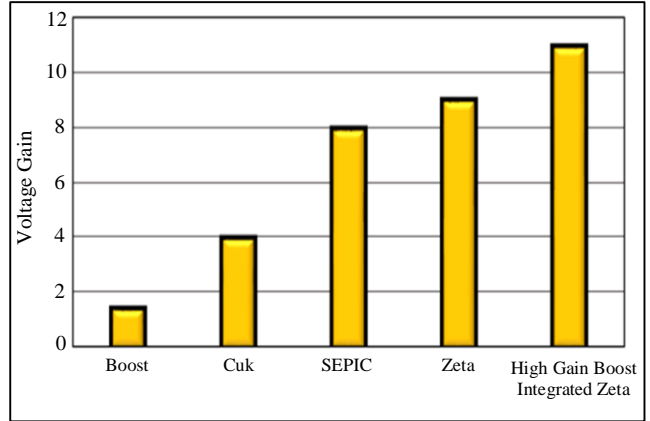


Fig. 18 Voltage gain comparison

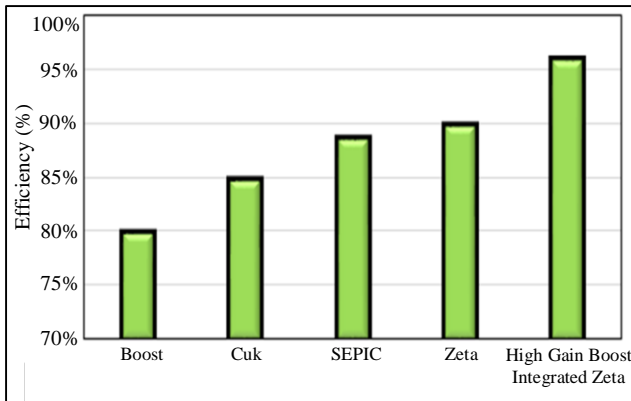


Fig. 17 Efficiency comparison

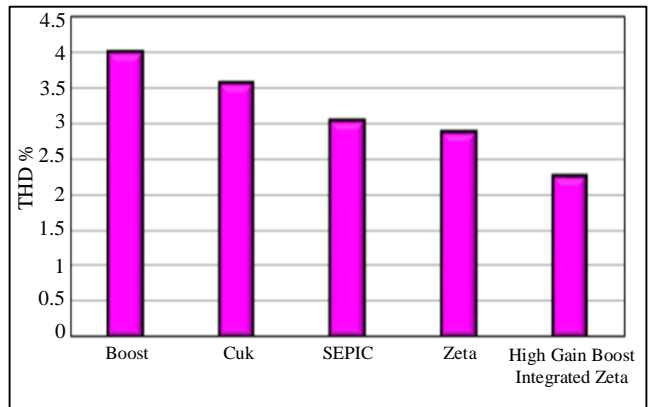


Fig. 19 THD comparison

**Table 2. Comparison analysis of efficiency**

Converters	Efficiency (%)
Boost	80 [21]
Cuk	85 [22]
SEPIC	88.82 [23]
Zeta	90 [24]
High gain boost integrated Zeta	96

**Table 3. Comparison analysis of controller**

Controller	Parameter		
	Rise Time ( $t_r$ )	Peak Time ( $t_p$ )	Settling Time ( $t_s$ )
PI	0.2 s	0.01 s	-
IMFO-PI	0.01 s	0.01 s	0.26 s

Table 2 examines the high gain Boost integrated Zeta converter's performance compared to the other prevalent converters. Here, the suggested converter's efficiency and voltage gain value of 96% & 1:1.1 are significantly higher than that of the other converters, and the corresponding plots are represented in Figures 17 and 18. As a result, it is demonstrated that the proposed converter has a significantly greater overall effectiveness than the others.

Table 3 represents the comparison analysis of the controller. The suggested research using the control technique gives better values for rise time ( $t_r$ ), peak time ( $t_p$ ), and

settling time ( $t_s$ ). Compared with ordinary PI controllers, the optimized PI controller has a faster settling time of 0.26 sec. Figure 19 indicates the THD comparison of the proposed converter; from the graph, it is evident that the proposed system has a minimized THD value of 2.25%.

## 6. Conclusion

This study describes an IoT-powered PV system with an EV. Battery system architecture that incorporates a unique high gain Boost integrated Zeta converter and an IMF-optimized PI controller. The proposed boost integrated converter is constructed with a single switch that minimizes its circuit and offers better regulation. With the implementation of this optimized PI controller, a better error companion with enhanced converter working operation is achieved. Furthermore, the entire system is observed in real-time through IoT to gain important information into usage designs that can then be used to optimize energy generation and consumption. Additionally, the excellence of the proposed technique is supported by comparison to other recently published methods. Furthermore, the Boost Integrated KY converter is expected to have an optimal efficiency of 96%, which is significantly more significant than other converters.

## Author Contributions

Ramani R.: Conceptualization, Data Curation, Methodology, and Writing original draft. Nalini A.: Methodology and Validation. Nalini A. & Ramani R.: Writing-review & editing.

## References

- [1] Tripura Pidikiti et al., "Design and Control of Takagi-Sugeno-Kang Fuzzy Controller Based Inverter for Power Quality Improvement in Grid-Tied PV Systems," *Measurement: Sensors*, vol. 25, pp. 1-7, 2023. [[CrossRef](#)] [[Google Scholar](#)] [[Publisher Link](#)]
- [2] Bhim Singh et al., "Implementation of Solar PV-Battery and Diesel Generator Based Electric Vehicle Charging Station," *IEEE Transactions on Industry Applications*, vol. 56, no. 4, pp. 4007-4016, 2020. [[CrossRef](#)] [[Google Scholar](#)] [[Publisher Link](#)]
- [3] Qin Yan, Bei Zhang, and Mladen Kezunovic, "Optimized Operational Cost Reduction for an EV Charging Station Integrated with Battery Energy Storage and PV Generation," *IEEE Transactions on Smart Grid*, vol. 10, no. 2, pp. 2096-2106, 2018. [[CrossRef](#)] [[Google Scholar](#)] [[Publisher Link](#)]
- [4] Marco Bindi et al., "Machine Learning-Based Monitoring of DC-DC Converters in Photovoltaic Applications," *Algorithms*, vol. 15, no. 3, pp. 1-18, 2022. [[CrossRef](#)] [[Google Scholar](#)] [[Publisher Link](#)]
- [5] K. Jyotheeswara Reddy, and N. Sudhakar, "High Voltage Gain Interleaved Boost Converter with Neural Network Based MPPT Controller for Fuel Cell Based Electric Vehicle Applications," *IEEE Access*, vol. 6, pp. 3899-3908, 2018. [[CrossRef](#)] [[Google Scholar](#)] [[Publisher Link](#)]
- [6] José-Enrique Hernández-Díez et al., "A Current Sensorless Delay-Based Control Scheme for MPPT-Boost Converters in Photovoltaic Systems," *IEEE Access*, vol. 8, pp. 174449-174462, 2020. [[CrossRef](#)] [[Google Scholar](#)] [[Publisher Link](#)]
- [7] Balaji Chandrasekar et al., "Non-Isolated High-Gain Triple Port DC-DC Buck-Boost Converter with Positive Output Voltage for Photovoltaic Applications," *IEEE Access*, vol. 8, pp. 113649-113666, 2020. [[CrossRef](#)] [[Google Scholar](#)] [[Publisher Link](#)]
- [8] Maria I.S. Guerra et al., "Assessing Maximum Power Point Tracking Intelligent Techniques on a PV System with a Buck-Boost Converter," *Energies*, vol. 14, no. 22, pp. 1-21, 2021. [[CrossRef](#)] [[Google Scholar](#)] [[Publisher Link](#)]
- [9] Neeraj Priyadarshi et al., "New CUK-SEPIC Converter Based Photovoltaic Power System with Hybrid GSA-PSO Algorithm Employing MPPT for Water Pumping Applications," *IET Power Electronics*, vol. 13, no. 13, pp. 2824-2830, 2020. [[CrossRef](#)] [[Google Scholar](#)] [[Publisher Link](#)]
- [10] Neeraj Priyadarshi et al., "Performance Evaluation of Solar-PV-Based Non-Isolated Switched-Inductor and Switched-Capacitor High-Step-Up Cuk Converter," *Electronics*, vol. 11, no. 9, pp. 1-17, 2022. [[CrossRef](#)] [[Google Scholar](#)] [[Publisher Link](#)]

- [11] P. Sivaraman, and C. Sharmeela, *IoT-Based Battery Management System for Hybrid Electric Vehicle*, Artificial Intelligent Techniques for Electric and Hybrid Electric Vehicles, pp. 1-16, 2020. [[CrossRef](#)] [[Google Scholar](#)] [[Publisher Link](#)]
- [12] Shabana Urooj et al., "IoT Based Electric Vehicle Application Using Boosting Algorithm for Smart Cities," *Energies*, vol. 14, no. 4, pp. 1-16, 2021. [[CrossRef](#)] [[Google Scholar](#)] [[Publisher Link](#)]
- [13] George F. Savari et al., "Internet of Things Based Real-Time Electric Vehicle Load Forecasting and Charging Station Recommendation," *ISA Transactions*, vol. 97, pp. 431-447, 2020. [[CrossRef](#)] [[Google Scholar](#)] [[Publisher Link](#)]
- [14] Bhim Singh et al., "Implementation of Solar PV-Battery and Diesel Generator Based Electric Vehicle Charging Station," *IEEE Transactions on Industry Applications*, vol. 56, no. 4, pp. 4007-4016, 2020. [[CrossRef](#)] [[Google Scholar](#)] [[Publisher Link](#)]
- [15] Barathi K., and P.K. Dhal, "PI Optimized Cuckoo Search Algorithm for Single Phase Grid Tied PV Inverter with SEPIC Converter," *Mathematical Modelling of Engineering Problems*, vol. 9, no. 1, 2022. [[CrossRef](#)] [[Google Scholar](#)] [[Publisher Link](#)]
- [16] Maher G.M. Abdolrasol et al., "Optimal PI Controller Based PSO Optimization for PV Inverter Using SPWM Techniques," *Energy Reports*, vol. 8, pp. 1003-1011, 2022. [[CrossRef](#)] [[Google Scholar](#)] [[Publisher Link](#)]
- [17] D.C. Meena, and Ambrish Devanshu, "Genetic Algorithm Tuned PID Controller for Process Control," *2017 International Conference on Inventive Systems and Control (ICISC)*, India, 2017. [[CrossRef](#)] [[Google Scholar](#)] [[Publisher Link](#)]
- [18] Aliyu Hamza Sule et al., "Optimal Tuning of Proportional Integral Controller for Fixed-Speed Wind Turbine Using Grey Wolf Optimizer," *International Journal of Electrical and Computer Engineering*, vol. 10, no. 5, pp. 5251-5261, 2020. [[CrossRef](#)] [[Google Scholar](#)] [[Publisher Link](#)]
- [19] Zhi Qi, Qian Shi, and Hui Zhang, "Tuning of Digital PID Controllers Using Particle Swarm Optimization Algorithm for a CAN-Based DC Motor Subject to Stochastic Delays," *IEEE Transactions on Industrial Electronics*, vol. 67, no. 7, pp. 5637-5646, 2019. [[CrossRef](#)] [[Google Scholar](#)] [[Publisher Link](#)]
- [20] Ali Q. Al-Shetwi et al., "Active Power Control to Mitigate Frequency Deviations in Large-Scale Grid-Connected PV System Using Grid-Forming Single-Stage Inverters," *Energies*, vol. 15, no. 6, pp. 1-21, 2022. [[CrossRef](#)] [[Google Scholar](#)] [[Publisher Link](#)]
- [21] Farzam Nejabatkhah et al., "Modeling and Control of a New Three-Input DC-DC Boost Converter for Hybrid PV/FC/Battery Power System," *IEEE Transactions on Power Electronics*, vol. 27, no. 5, pp. 2309-2324, 2021. [[CrossRef](#)] [[Google Scholar](#)] [[Publisher Link](#)]
- [22] Francarl Galea et al., "Design of A High Efficiency Wide Input Range Isolated Cuk DC-DC Converter for Grid Connected Regenerative Active Loads," *World Engineers' Convention*, Geneva, pp. 1-11, 2011. [[Google Scholar](#)] [[Publisher Link](#)]
- [23] Patan Javeed et al., "SEPIC Converter for Low Power LED Applications," *Journal of Physics: Conference Series*, vol. 1818, pp. 1-12, 2021. [[CrossRef](#)] [[Google Scholar](#)] [[Publisher Link](#)]
- [24] S. Saravanan, P. Usha Rani, and M.P. Thakre, "Evaluation and Improvement of a Transformerless High-Efficiency DC-DC Converter for Renewable Energy Applications Employing A Fuzzy Logic Controller," *MAPAN-Journal Metrology Society of India*, vol. 37, pp. 291-310, 2022. [[CrossRef](#)] [[Google Scholar](#)] [[Publisher Link](#)]